



# Adsorption and dissociation of O<sub>2</sub> on the Cu<sub>2</sub>O(1 1 1) surface: Thermochemistry, reaction barrier

Riguang Zhang, Hongyan Liu, Huayan Zheng, Lixia Ling, Zhong Li, Baojun Wang\*

Key Laboratory of Coal Science and Technology of Ministry of Education and Shanxi Province, Taiyuan University of Technology, No. 79 Yingze West Street, Taiyuan 030024, Shanxi, China

## ARTICLE INFO

### Article history:

Received 11 October 2010

Accepted 7 December 2010

Available online 17 December 2010

### Keywords:

Oxygen

Cu<sub>2</sub>O(1 1 1)

Adsorption

Dissociation

Density functional theory

## ABSTRACT

The adsorption and dissociation of O<sub>2</sub> on the perfect and oxygen-deficient Cu<sub>2</sub>O(1 1 1) surface have been systematically studied using periodic density functional calculations. Different kinds of possible modes of atomic O and molecular O<sub>2</sub> adsorbed on the Cu<sub>2</sub>O(1 1 1) surface are identified: atomic O is found to prefer threefold 3Cu site on the perfect surface and O<sub>vacancy</sub> site on the deficient surface, respectively. Cu<sub>CUS</sub> is the most advantageous site with molecularly adsorbed O<sub>2</sub> lying flatly over singly coordinate Cu<sub>CUS</sub>–Cu<sub>CSA</sub> bridge on the perfect surface. O<sub>2</sub> adsorbed dissociatively on the deficient surface, which is the main dissociation pathway of O<sub>2</sub>, and a small quantity of molecularly adsorbed O<sub>2</sub> has been obtained. Further, possible dissociation pathways of molecularly adsorbed O<sub>2</sub> on the Cu<sub>2</sub>O(1 1 1) surface are explored, the reaction energies and relevant barriers show that a small quantity of molecularly adsorbed O<sub>2</sub> dissociation into two O atoms on the deficient surface is favorable both thermodynamically and kinetically in comparison with the dissociation of O<sub>2</sub> on the perfect surface. The calculated results suggest that the presence of oxygen vacancy exhibits a strong chemical reactivity towards the dissociation of O<sub>2</sub> and can obviously improve the catalytic activity of Cu<sub>2</sub>O, which is in agreement with the experimental observation.

© 2010 Elsevier B.V. All rights reserved.

## 1. Introduction

Cu<sup>+</sup> ions have been postulated to be the active species for the formation of dimethyl carbonate (DMC) by the oxidative carbonylation of methanol [1–3]. To avoid equipment corrosion and catalyst deactivation, Cu<sub>2</sub>O has been chosen as a chlorine-free and ideal model system to investigate the catalytic mechanism for the oxidative carbonylation of methanol to DMC [4,5]. In our experimental work [6,7], the chlorine-free catalyst Cu<sub>2</sub>O/AC by dipping Cu(CH<sub>3</sub>COO)<sub>2</sub> onto activated carbon (AC) surface has been prepared, the Cu<sub>2</sub>O/AC catalyst performs a good catalytic activity for the oxidative carbonylation of methanol, in which Cu<sub>2</sub>O has been postulated to be the catalytic active species. Bulk Cu<sub>2</sub>O lattice has cuprite (Pn3) cubic structure in which each oxygen is at the center of a tetrahedron of copper atoms linearly coordinated with two oxide ions [8]. The bulk-terminated Cu<sub>2</sub>O(1 1 1) surface possesses hexagonal symmetry and planes parallel to the surfaces containing either copper cations or oxygen anions. The geometric and electrical structure of Cu<sub>2</sub>O(1 1 1) have been investigated experimentally by Schulz and Cox [9] using low energy electron diffraction (LEED) and X-ray and ultra-violet photoelectron spec-

troscopy. Since Cu<sub>2</sub>O(1 1 1) surface is non-polar and stable [10], it has been the subject of several experimental and theoretical investigations [9,11–17], which have focused on understanding its surface structure and the characteristics of adsorption of gases such as H<sub>2</sub>, CO and NO.

Up to now, many studies about the mechanism of DMC synthesis over CuCl catalyst or Cu-exchanged zeolites have shown that the interaction of CH<sub>3</sub>OH, CH<sub>3</sub>O, CO and O<sub>2</sub> with CuCl catalyst and Cu-exchanged zeolites is of great significance to study the mechanism and kinetics of DMC synthesis [1–3,5,18–21]. Consequently, for the DMC synthesis over Cu<sub>2</sub>O catalyst, a detail about the interaction of CH<sub>3</sub>OH, CH<sub>3</sub>O, CO and O<sub>2</sub> with Cu<sub>2</sub>O is very important to understand the structure of Cu<sub>2</sub>O and the catalytic mechanism of this process. In our previous studies [22], CO and CH<sub>3</sub>O adsorption and co-adsorption on the Cu<sub>2</sub>O(1 1 1) surface have been systematically investigated, which suggests that the adsorption of CO and CH<sub>3</sub>O can effectively improve the relaxation of Cu<sub>2</sub>O(1 1 1) surface, and the interaction between CO and CH<sub>3</sub>O favors the formation of CH<sub>3</sub>OCO.

Meanwhile, since the adsorption of gas-phase oxygen at oxide surfaces plays an important role in many types of heterogeneous catalysis [23–25], the adsorption and dissociation of O<sub>2</sub> on the Cu<sub>2</sub>O(1 1 1) surface is a central component of the catalytic activity of Cu<sub>2</sub>O in DMC synthesis. Although experiments by Schulz and Cox [9] have investigated the adsorption of O<sub>2</sub> on the perfect and

\* Corresponding author. Tel.: +86 351 6018539; fax: +86 351 6041237.

E-mail address: [wangbaojun@tyut.edu.cn](mailto:wangbaojun@tyut.edu.cn) (B. Wang).

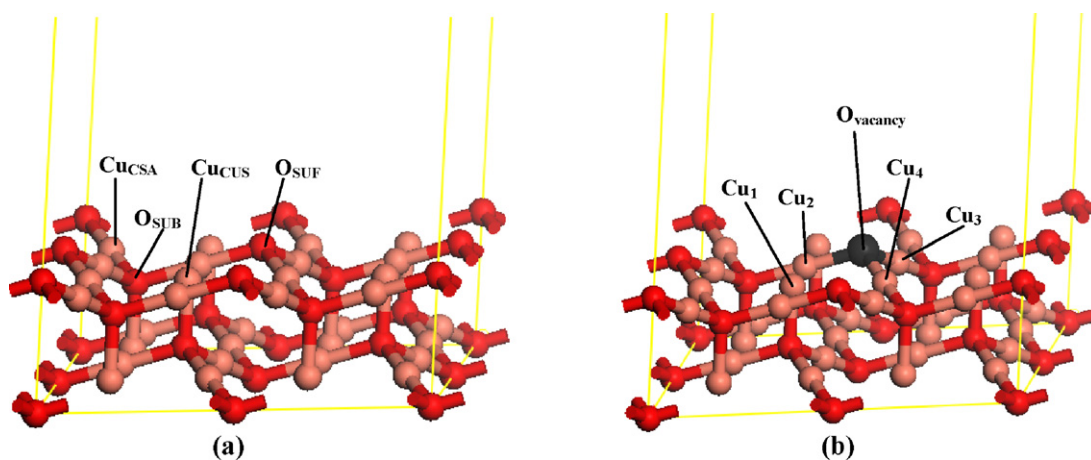


**Fig. 1.** The slab model of  $\text{Cu}_2\text{O}(111)-(2 \times 2)$ . (a) Perfect  $\text{Cu}_2\text{O}(111)$  surface; (b) oxygen-deficient  $\text{Cu}_2\text{O}(111)$  surface. Orange and red balls stand for Cu and O atoms and black ball stands for oxygen vacancy site. (For interpretation of the references to color in this figure legend, the reader is referred to the web version of the article.)

oxygen-deficient  $\text{Cu}_2\text{O}(111)$  surfaces, the position and behavior of  $\text{O}_2$  and the resultant atomic O is less well understood. Meanwhile, the difference between adsorbed and lattice oxygen is hardly distinguished, unless the adsorbed species carry a net spin, through isotope-exchange experiments [26,27] are an exception to this. Spin-resonance experiments have given firm evidence for adsorbed oxygen species such as  $\text{O}^-$  and  $\text{O}_2^-$  on some oxide surfaces but there is only rather weak evidence for other potentially important species such as  $\text{O}_2^{2-}$  [25,28]. Therefore, for a detailed understanding of the surface process, experimental information is however not always sufficient and accompanying theoretical calculations can be helpful to clarify some questions. With recent developments, density functional theory (DFT) method has already been extensively used to provide qualitative and quantitative insights into the structure of active surfaces and surface reaction [25,29–35]. Nowadays, several theoretical studies of  $\text{O}_2$  adsorption on metal oxide surface  $\text{MgO}(001)$  [25,34],  $\text{SnO}_2(110)$  [35],  $\text{Cu}_2\text{O}(100)$  [10],  $\text{La}_2\text{O}_3(001)$  [36] and  $\text{TiO}_2(110)$  [37,38] have been reported. To the best of our knowledge, few theoretical studies about the  $\text{O}_2$  adsorption on the  $\text{Cu}_2\text{O}(111)$  surfaces have been systematically reported, which will be helpful to deeply probe into the adsorption geometry and behavior of atomic oxygen and molecular oxygen on the  $\text{Cu}_2\text{O}(111)$  surface, reaction barrier and the role of the surface defect at a microscopic level. Only Sun et al. [39] investigated the interaction of  $\text{O}_2$  with the fixed  $\text{Cu}_2\text{O}(111)$  surface by DFT method, however,  $\text{Cu}_2\text{O}(111)$  surface exhibits relaxation in experiment [40–42]. Further, previous studies about the adsorption of  $\text{H}_2$ , CO and NO on the  $\text{Cu}_2\text{O}(111)$  surface [11,14–17] have shown that the relaxation of  $\text{Cu}_2\text{O}(111)$  surface should be considered.

In this study, taking the relaxation of  $\text{Cu}_2\text{O}(111)$  surface into consideration, we pay particular attention to understanding  $\text{Cu}_2\text{O}$  catalyzed adsorption and dissociation of oxygen. The first-principles density functional theory (DFT) and self-consistent periodic calculation are applied to systematically investigate the adsorption energies and adsorption geometries of the atomic and molecular oxygen on the relaxed  $\text{Cu}_2\text{O}(111)$  surface, the reaction energies and relevant barriers for the dissociation of  $\text{O}_2$  on the relaxed  $\text{Cu}_2\text{O}(111)$  surface, as well as the role of the oxygen vacancy on this surface, which may be of interest to researchers attempting to illustrate the catalytic mechanism for the formation of DMC by the oxidative carbonylation of methanol.

## 2. Computational models and methods

### 2.1. Surface models

Based on the structure of bulk  $\text{Cu}_2\text{O}$ ,  $\text{Cu}_2\text{O}(111)$  surface were modeled by using the supercell approach, where periodic boundary condition are applied to the central supercell so that it is reproduced periodically throughout space. The perfect  $\text{Cu}_2\text{O}(111)$  surface is non-polar including four chemically different types of surface atoms, which were denoted as  $\text{Cu}_{\text{CUS}}$ ,  $\text{Cu}_{\text{CSA}}$ ,  $\text{O}_{\text{SUF}}$  and  $\text{O}_{\text{SUB}}$  (see Fig. 1(a)).  $\text{Cu}_{\text{CUS}}$  is the surface copper that is coordinatively unsaturated, i.e., singly coordinate  $\text{Cu}^+$  cations.  $\text{Cu}_{\text{CSA}}$  is the coordinatively saturated copper atom, i.e., doubly coordinate  $\text{Cu}^+$ .  $\text{O}_{\text{SUF}}$  is the outer-most surface oxygen, i.e., threefold-coordinate oxygen anions.  $\text{O}_{\text{SUB}}$  is the subsurface oxygen, i.e. fourfold-coordinate oxygen anions. The removal of the oxygen of top atomic layer from the perfect surface results in what is called the oxygen-deficient  $\text{Cu}_2\text{O}(111)$  surface [16], as presented in Fig. 1(b). Each oxygen vacancy gives rise to a threefold site of singly coordinate  $\text{Cu}^+$  cations (i.e.,  $\text{Cu}_2$ ,  $\text{Cu}_3$  and  $\text{Cu}_4$  atoms as labeled in Fig. 1(b)).

Our calculations on the perfect  $(2 \times 2)$  and oxygen-deficient  $(2 \times 2)$  surfaces have been done by using slab models of six atomic layers. Adsorbate and the three outermost atomic layers of the substrate were allowed to relax in all of the geometry optimization calculations (allowed to move in any direction according to forces), and the three bottom-most atomic layers of the substrate were kept fixed to the bulk coordinates. A vacuum layer of 10 Å along the z-direction perpendicular to the surface (x and y being parallel) was employed to prevent spurious interactions between the repeated slabs.

### 2.2. Calculation methods

In our study, DFT has been employed to perform for all calculations. This approach allows us to study rather large periodic systems, so that the adsorbed species are present at low coverage, while we avoid the well-known boundary effects associated with cluster calculations. The choice of exchange-correlation functional is a crucial issue for surface calculation. Generalized gradient approximations (GGA) can give very much better dissociation energies [43] and are now widely used in molecular calculations; there is strong evidence that they also give much better adsorption energies [44]. The main calculations present here are based on the

GGA of Becke–Lee–Yang–Parr (BLYP) exchange–correlation functional [45,46]. In the computation, the inner electrons of copper atoms were kept frozen and replaced by an effective core potential (ECP) [47,48], and oxygen atoms were treated with an all-electron basis set. The valence electrons functions were expanded into a set of numerical atomic orbitals by a double-numerical basis with polarization functions (DNP) [49]. Brillouin-zone integrations have been performed using  $2 \times 2 \times 1$  Monkhorst–Pack grid and a Methfessel–Paxton smearing of 0.005 Ha.

In order to determine accurate activation energies of  $O_2$  dissociation, we chose Complete LST/QST approach to search for the transition states of reactions [50], starting from reactants and products, the LST (Linear Synchronous Transit) method performs a single interpolation to a maximum energy, and the QST (Quadratic Synchronous Transit) method alternates searches for an energy maximum with constrained minimizations in order to refine the transition state to a high degree. All calculations were carried out with the Dmol<sup>3</sup> program package in Materials Studio 4.4 [51,52] on HP Proliant DL 380 G5 server system.

### 3. Results and discussion

#### 3.1. Calculations of $O_2$ molecule and bulk $Cu_2O$

The bond length of molecular  $O_2$  calculated from our approach are  $r(O-O) = 0.124$  nm, in good agreement with the experimental values of 0.121 nm [53], as well as to other similar GGA results [9]. Then, the test was to predict the lattice constant of bulk  $Cu_2O$ . The calculated value for the lattice constant is 0.4430 nm in comparison with the experimental value of 0.4270 nm [5,54]. Above results obtained in these tests made us confident in pursuing the next step of our investigations, namely the interaction of O and  $O_2$  with  $Cu_2O$  surface.

#### 3.2. Atomic oxygen adsorption on the $Cu_2O(111)$ surface

The adsorption energy is always regarded as a measure of the strength of adsorbate–substrate adsorption. The adsorption energies are calculated using the expression  $E_{ads} = E_{sub} + E_{mol} - E_{mol/sub}$ , where  $E_{mol/sub}$  is the total energy of adsorbate–substrate system in its equilibrium state,  $E_{sub}$  is the energy of the substrate, and  $E_{mol}$  is the energy of the isolated adsorbate. With this definition, positive value of adsorption energy denotes that adsorption is more stable than the corresponding substrate and free adsorbate. The atomic or molecular oxygen entering this definition is in the true (triplet) ground state, irrespective of whether the adsorbed system is in the single or triplet state.

**Table 1**

Calculated adsorption properties for atomic oxygen adsorption on the  $Cu_2O(111)$  surface.

Sites	$d(O-Cu_{CUS})$ (nm)	$d(O-O_{SUF})$ (nm)	$d(O-Cu_{CSA})$ (nm)	$q(O)$	$E_{ads}$ ( $kJ\ mol^{-1}$ )
3Cu	0.1846		0.2043 (0.2044)	-0.514	349.6
$O_{SUF}$		0.098		-0.363	81.6
$O_{vacancy}$			0.1860 (0.1860, 0.1862)	-0.505	571.1

The adsorption of atomic oxygen on the  $Cu_2O(111)$  surface are calculated at a coverage of 1/4 ML with one atomic oxygen in every ( $2 \times 2$ ) unit cell. Five distinct adsorption sites presented in Fig. 1(a) and (b) are examined. In the case of atomic O adsorption at  $Cu_{CUS}$ ,  $Cu_{CSA}$ ,  $O_{SUB}$  and  $O_{SUF}$  sites, the perfect surface is employed to calculations, while in the case of  $O_{vacancy}$  site, the oxygen-deficient surface is employed to calculations. The adsorption energies and the equilibrium distances between atomic O and surface adsorption sites are listed in Table 1.

From the calculated adsorption energies listed in Table 1, in the case of O adsorbed over the perfect surface, the optimized configuration of O adsorbed at  $O_{SUF}$  site still bounds to  $O_{SUF}$  site. And the configurations at  $Cu_{CUS}$ ,  $Cu_{CSA}$  and  $O_{SUB}$  sites are then optimized but the O adsorbed all bounds to three Cu atoms, i.e., one  $Cu_{CUS}$  and two  $Cu_{CSA}$  (seen in Fig. 2(a), in this study the site consisting of one  $Cu_{CUS}$  and two  $Cu_{CSA}$  is defined as 3Cu site), which reflects the important contribution from the nearby cations. In the case of  $O_{vacancy}$  site, the vacancy site is filled with atomic O (as shown in Fig. 2(b)). Above calculation results show that 3Cu and  $O_{vacancy}$  sites are the most stable sites on the perfect and oxygen-deficient  $Cu_2O(111)$  surface, respectively, suggesting that 3Cu and  $O_{vacancy}$  sites are the active centers for atomic O adsorbed on the  $Cu_2O(111)$  surface, and the corresponding Mulliken population analysis also indicates that the charges transfer from  $Cu_2O(111)$  surface to atomic O.

According to the calculated adsorption energies, we suspect that there may be four products for the dissociation of  $O_2$  into two O atoms on the  $Cu_2O(111)$  surface. For the perfect surface, one is called P1, i.e., two atomic O are adsorbed at two adjacent 3Cu sites, respectively, the other is called P2, i.e., one atomic O is adsorbed at 3Cu site and the other bounds to the close  $O_{SUF}$  site. For the deficient surface, one is called P3, i.e., two atomic O are adsorbed at two adjacent 3Cu sites, respectively, the other is called P4, i.e., one atomic O is almost completely inserted into the crystal lattice and the other bounds to 3Cu site. The optimized structures of P1, P2, P3 and P4 are presented in Fig. 3.

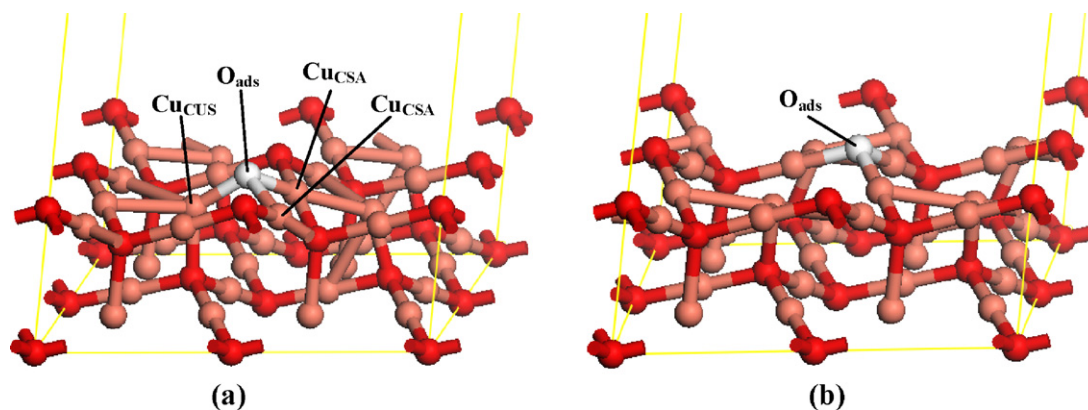


**Fig. 2.** Optimized configuration of atomic O coordinated at different adsorption sites. (a)  $Cu_{CUS}$ ,  $Cu_{CSA}$  and  $O_{SUB}$  sites; (b)  $O_{vacancy}$  site. Orange and red balls stand for Cu and O atoms of  $Cu_2O(111)$  substrate and white ball stands for O atom adsorbed on  $Cu_2O(111)$  surface throughout the paper, respectively. (For interpretation of the references to color in this figure legend, the reader is referred to the web version of the article.)

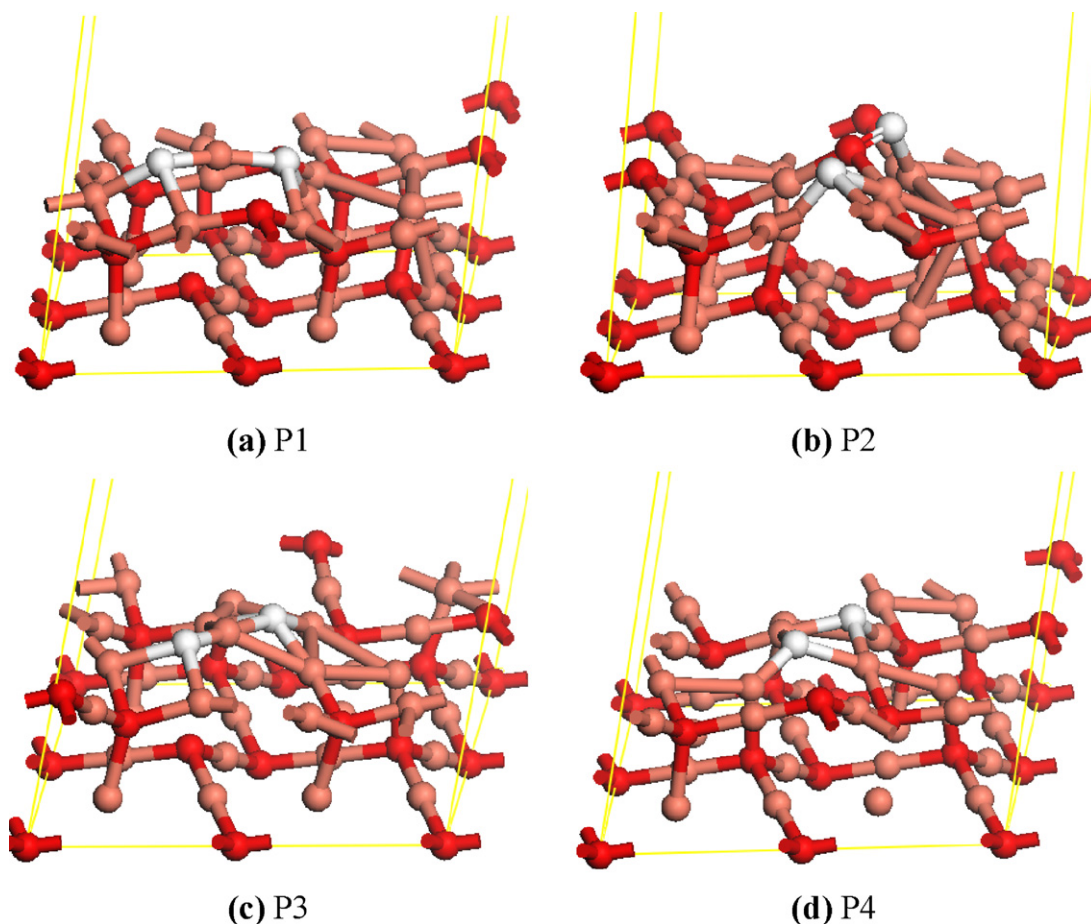


Fig. 3. Optimized geometric structures of (a) P1, (b) P2, (c) P3 and (d) P4.

### 3.3. $O_2$ adsorption on the perfect $Cu_2O(111)$ surface

Calculations for  $O_2$  adsorption on the perfect surface are carried out at a coverage of  $1/4$  ML with one molecule in every  $(2 \times 2)$  unit cell,  $O_2$  is allowed to approach the perfect surface along two adsorption modes over the four distinct sites, in which the molecular axis of  $O_2$  is either perpendicular or parallel to the surface, as presented in Fig. 4. The calculated results show that the adsorption structure of the triplet state is more stable than that of the single state, so only the adsorption energies, bond lengths, Mulliken charges and stretching frequencies of  $O_2$  in a triplet state are summarized in Table 2.

According to Table 2, it is interesting to find that adsorption of molecular  $O_2$  is less favorable than that of atomic O. For the

perpendicular M1 mode, the optimized structure converts to the model with  $O_2$  lying flatly over singly coordinate  $Cu_{CUS}-Cu_{CSA}$  bridge (seen in Fig. 5), which is the most stable adsorption structure with the largest adsorption energy of  $56.3 \text{ kJ mol}^{-1}$ , and the corresponding O–O bond length of adsorbed  $O_2$  is elongated to  $0.1390 \text{ nm}$  from  $0.1236 \text{ nm}$  in free  $O_2$  molecule. The Mulliken charges show that electron transfer from substrate to  $O_2$  is  $0.481 e$ . For the parallel M5 mode, the optimized structure is similar with the optimized M1, the O–O bond length is  $0.1385 \text{ nm}$ , and the corresponding adsorption energy is  $56.2 \text{ kJ mol}^{-1}$ . In the optimized M2 and M4 modes, although  $O_2$  still bounds to  $Cu_{CSA}$  and  $O_{SUB}$  sites, respectively, the corresponding adsorption energies are negative; this suggests that the adsorption of  $O_2$  in M2 and M4 modes is not thermodynamically favored. For the optimized M6 and M8 modes,

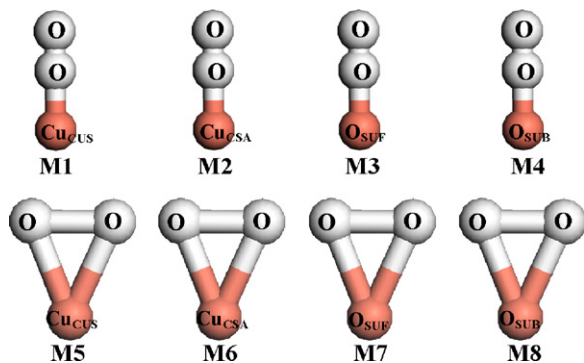
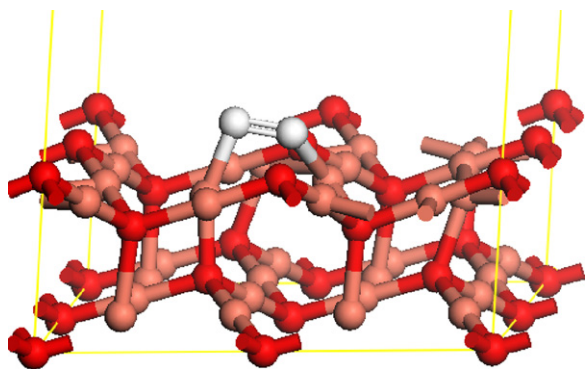


Fig. 4. Adsorption geometries of  $O_2$  adsorbed on the perfect  $Cu_2O(111)$  surface.

Table 2

Properties of  $O_2$  adsorbed at different sites on the perfect  $Cu_2O(111)$  surface.

Adsorption mode	$r(O-O)$ (nm)	$q(O_2)$	$E_{ads}$ ( $\text{kJ mol}^{-1}$ )	$\nu(O-O)$ ( $\text{cm}^{-1}$ )
M1	0.1390	-0.481	56.3	876.4
M2	0.1287	-0.255	-38.0	
M3	0.1245	-0.063	7.9	
M4	0.1285	-0.258	-44.1	
M5	0.1385	-0.421	56.2	887.5
M6	0.1377	-0.401	36.2	
M7	0.1244	-0.065	0.8	
M8	0.1381	-0.406	35.3	
Free $O_2$	0.1236			1493.5
$O_2^-$ [39,55]	0.1280			~1097
$O_2^{2-}$ [39,55]	0.1490			~766



**Fig. 5.** Optimized geometric structures of  $O_2$  adsorbed at  $Cu_{CUS}$  site on the perfect  $Cu_2O(111)$  surface. Orange and red balls stand for Cu and O atoms in  $Cu_2O(111)$  substrate and two white balls stand for  $O_2$  adsorbed on  $Cu_2O(111)$  surface throughout the paper, respectively. (For interpretation of the references to color in this figure legend, the reader is referred to the web version of the article.)

$O_2$  also converts to the model with  $O_2$  lying flatly over singly coordinate  $Cu_{CUS}$ – $Cu_{CSA}$  bridge, in which the O–O bond length of adsorbed  $O_2$  are 0.1377 and 0.1381 nm, respectively, and the corresponding adsorption energies are 36.2 and 35.3  $\text{kJ mol}^{-1}$ , respectively. In the optimized M3 and M7 modes,  $O_2$  is far above the surface, and the corresponding adsorption energies vary little with adsorption site and orientation, the O–O bond lengths of adsorbed  $O_2$  molecules change little with respect to free  $O_2$  molecule.

Above results show that for M1 and M5 modes they are chemisorption ( $E_{\text{ads}} > 40 \text{ kJ mol}^{-1}$ ),  $O_2$  molecularly adsorbed on the perfect  $Cu_2O(111)$  surface, which accords with the experimental results about  $O_2$  adsorbed on the perfect  $Cu_2O(111)$  surface by Schulz and Cox [9]. The structural changes of the optimized M1 and M5 modes suggest that  $O_2$  adsorbed molecularly on the perfect surface are likely precursors to  $O_2$  dissociation, in which their molecular axes are parallel to the surface (the di- $\sigma$  configuration).  $Cu_{CUS}$  is thought to be the advantageous active site on the perfect  $Cu_2O(111)$  surface, which mainly contributes to the dissociation of  $O_2$ .

In addition, vibrational spectroscopy has suggested the existence of a peroxo form ( $O_2^{2-}$ ), with a stretching frequency of  $\sim 766 \text{ cm}^{-1}$ , and a superoxo ( $O_2^-$ ) form, with a stretching frequency of  $\sim 1097 \text{ cm}^{-1}$ . As listed in Table 2, for the optimized M1 and M5 modes, the  $\nu(O_2)$  distributes over a range from 876.4 to 887.5  $\text{cm}^{-1}$ , the O–O bond length of adsorbed  $O_2$  (0.1385–0.1390 nm) is close to that of the  $O_2^{2-}$  ion (0.1490 nm), which means that the oxygen species attribute to the characteristic of  $O_2^{2-}$  form; all of these indicate that the oxygen species adsorbed on the perfect surface mainly exist in the form of  $O_2^{2-}$  type. Although there are no experimental data available for comparison with our calculated results, the calculated vibrational frequencies can serve as good indicators for future experiments in this area. A red-shift of the O–O bond stretching frequency is observed. The trend in vibrational frequency is consistent with that of the O–O bond length and Mulliken charges of adsorbed  $O_2$ . Namely, significant charge transfer from the substrate to the  $O_2$  can weaken the intensity of the O–O bond, causing it to lengthen and reducing its frequency.

#### 3.4. $O_2$ adsorption on the oxygen-deficient $Cu_2O(111)$ surface

Usually  $O_2$  does not dissociate on metal oxide surfaces unless vacancies are present, in order to understand the role of the vacancy, we studied the adsorption of  $O_2$  in a triplet state on the oxygen-deficient  $Cu_2O(111)$  surface at a coverage of 1/4 ML with one molecule in every  $(2 \times 2)$  unit cell. Admittedly, the geometric structures of  $Cu_2O(111)$ – $(2 \times 2)$  with 25% oxygen-vacancies (1/4 of

$O_{\text{SUR}}$  atoms were missing) is a large number of vacancies and may not depict reality, but the intention here is to obtain only a qualitative understanding of the oxygen-deficient surface. Meanwhile, above results show that  $Cu_{CUS}$  is the advantageous adsorption site. Thus herein, only two different kinds of catalytic active sites for the adsorption of  $O_2$  on the oxygen-deficient surface,  $Cu_{CUS}$  and  $O_{\text{vacancy}}$  sites, were investigated. Owing to the fact that Cu atoms nearby the  $O_{\text{vacancy}}$  site (i.e.,  $Cu_1$ ,  $Cu_2$ ,  $Cu_3$  and  $Cu_4$  atoms annotated in Fig. 1(b)) are all singly coordination, these Cu atoms belong to the same kind. Therefore, for the adsorption of  $O_2$  on the deficient surface, seven adsorption modes around oxygen-vacancy have been considered, as illustrated in Fig. 6. (a)  $O_2$  lies flatly over the  $Cu_1$ – $Cu_3$  bridge site; (b)  $O_2$  lies flatly over  $Cu_2$ – $Cu_4$  bridge site; (c)  $O_2$  lies flatly over the  $Cu_1$ –vacancy bridge site; (d)  $O_2$  is parallel to  $O_{\text{vacancy}}$  site; (e)  $O_2$  is parallel to  $Cu_1$  site; (f)  $O_2$  is perpendicular to  $O_{\text{vacancy}}$  site; (g)  $O_2$  is perpendicular to  $Cu_1$  site. The relevant adsorption energies, O–O bond distances and Mulliken charges of the optimized adsorption modes are listed in Table 3.

According to the results listed in Table 3, the optimized M(a) structure is very similar to the optimized M(c) and M(g) structures, which leads to the structure that one atomic oxygen is almost completely inserted into the crystal lattice and the other bounds to 3Cu site, as shown in Fig. 3(d). The optimized M(b) structure is that two atomic oxygen bound to the adjacent 3Cu site (see Fig. 3(c)). These results are consistent with the above results predicted from atomic oxygen adsorption on the  $Cu_2O(111)$  surfaces. In the optimized M(a)–M(c) and M(g) structures, the rather large distances of O–O bond (0.2559, 0.3212, 0.2541 and 0.2556 nm) indicate that the O–O bond has been completely broken. Namely, no activation energy is required for the dissociation of  $O_2$  into two O atoms on the deficient surface. For the M(d) and M(f) modes, the optimized structures show that  $O_2$  still bounds to the  $O_{\text{vacancy}}$  site, as shown in Fig. 7. For the M(e) mode, the optimized structure converts to the model with  $O_2$  lying flatly over singly coordinate  $Cu_{CUS}$ – $Cu_{CSA}$  bridge (see in Fig. 7). The O–O bond in the optimized M(d)–M(f) structures is 0.1550, 0.1401 and 0.1529 nm, respectively, which is stretched significantly compared to that in free  $O_2$  molecule (0.1236 nm). Despite of the elongation of the O–O bond, the O–O bond has not been broken according to the monitor bonding function of the Dmol<sup>3</sup>. However, these configurations can contribute to the dissociation of  $O_2$ , in which the dissociation processes of  $O_2$  virtually need to overcome an energy barrier. Moreover, the O–O bond length of adsorbed  $O_2$  (0.1401–0.1550 nm) for the optimized M(d)–M(f) structures is close to that of the  $O_2^{2-}$  ion (0.1490 nm), the  $\nu(O_2)$  distributes over a range from 619.0 to 850.7  $\text{cm}^{-1}$ , suggesting that the oxygen adspecies is characteristic of a classical  $O_2^{2-}$  ion on the oxygen-deficient surface.  $O_2$  molecule still carries negative charges and a red-shift of the O–O stretching frequency is observed.

Therefore, in the view of the O–O bond lengths and the adsorption energies, M(a)–M(c) and M(g) are the advantageous adsorption modes towards the dissociation of  $O_2$ , which are typical of dissociative adsorption modes. In other words, the dissociative adsorption is the main dissociation pathway of  $O_2$  on the deficient surface, which suggests that  $Cu_2O(111)$  surface with oxygen vacancy exhibits a strong chemical reactivity towards the dissociation of  $O_2$ . Moreover, Schulz and Cox [9] have investigated the adsorption of  $O_2$  on the deficient  $Cu_2O(111)$  surface in details by using LEED, XPS and UPS, the experimental results show  $O_2$  adsorbs dissociatively on the deficient surface under vacuum conditions, and the atomic oxygen show characteristics of both incorporated (i.e., lattice) and adsorbed oxygen. Our calculation results of  $O_2$  adsorption on the deficient surface are consistent with that of the experimental observations.

In addition, above calculated results also show that when the dissociative adsorption of  $O_2$  on the deficient surface for M(a)–M(c)

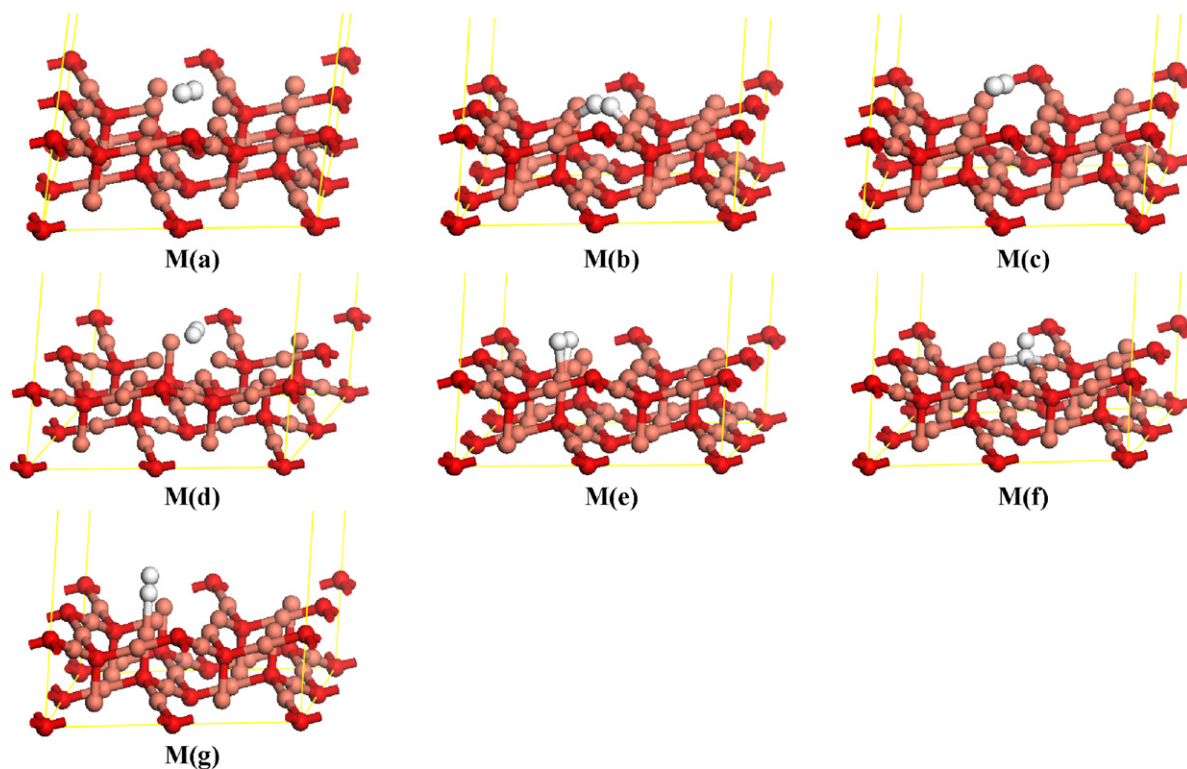


Fig. 6. Adsorption geometries of  $O_2$  adsorbed on the deficient  $Cu_2O(111)$  surface.

Table 3

Properties of  $O_2$  adsorbed on the oxygen-deficient  $Cu_2O(111)$  surface with different adsorption modes.

Adsorption mode	$r(O-O)$ (nm)	$q(O_2)$	$E_{ads}$ ( $kJ\ mol^{-1}$ )	$\nu(O-O)$ ( $cm^{-1}$ )
M(a)	0.2559	-0.961	330.4	
M(b)	0.3212	-1.054	367.6	
M(c)	0.2541	-0.958	328.2	
M(d)	0.1550	-0.594	176.3	619.0
M(e)	0.1401	-0.441	65.8	850.7
M(f)	0.1529	-0.585	163.8	679.7
M(g)	0.2556	-0.957	326.2	
Free $O_2$	0.1236			1493.5
$O_2^-$	0.1280			~1097
$O_2^{2-}$	0.1490			~766

and M(g) modes is occurring as a main dissociation pathway without any activation energy required, a small quantity of  $O_2$  dissociation reactions for M(d)–M(f) modes also occur, which need to overcome an energy barrier.

### 3.5. $O_2$ dissociation on the $Cu_2O(111)$ surface

To obtain further detailed understanding about the catalytic activity of  $Cu_{CUS}$  site on the perfect  $Cu_2O(111)$  surface in the section 3.3 and a small quantity of  $O_2$  dissociation for M(d)–M(f) modes on the deficient surface in the section 3.4, what to be investigated first is the dissociation of  $O_2$  at  $Cu_{CUS}$  site on the perfect surface. The dissociation of  $O_2$  on the perfect surface is also studied with one molecule in every  $(2 \times 2)$  unit cell. Thus the initial state represents a molecular coverage of 1/4 ML, leading to a dissociated final state with an atomic coverage of 1/2 ML. As the optimized M1 structure is the most stable geometry of the molecular  $O_2$  adsorption on the perfect  $Cu_2O(111)$  surface, the optimized M1 was naturally chosen as the initial reactant for the  $O_2$  dissociation, as described in Fig. 5, and the products P1 and P2 are chosen as the final product of this process, as presented in Fig. 3(a) and (b). Then, the dissociation of  $O_2$  on the deficient surface is calculated, in which the optimized M(d)–M(f) modes are chosen to be the initial reactants, respectively, as shown in Fig. 6(b), which

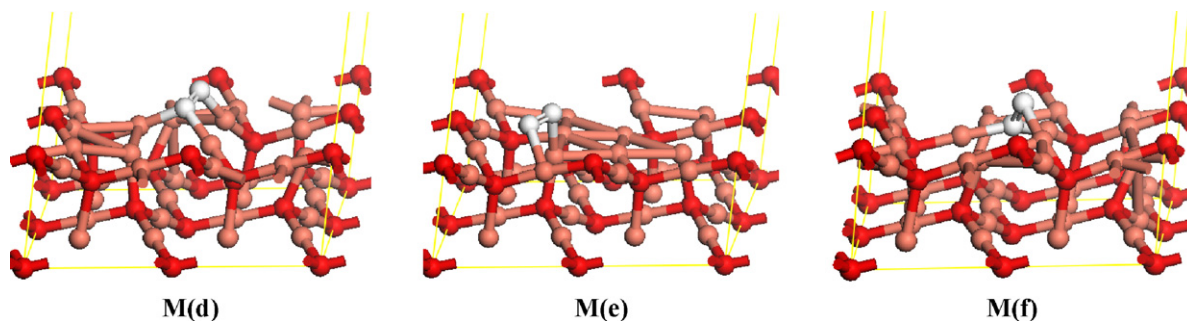


Fig. 7. Optimized geometric structures of the M(d)–M(f) adsorption modes.

**Table 4**  
Reaction energies ( $\Delta E$ ) and relevant barriers ( $E_a$ ) of  $O_2$  dissociation on the  $Cu_2O(111)$  surface.

Surface dissociation reaction	$E_a$ (kJ mol <sup>-1</sup> )	$\Delta E$ (kJ mol <sup>-1</sup> )
Perfect surface		
M1 → P1	123.1	-82.4
M1 → P2	164.9	84.8
Deficient surface		
M(d) → P3	82.4	-245.0
M(e) → P4	17.8	-209.4
M(f) → P4	12.8	-198.7

can results in the product P3 and P4 (see Fig. 3(c) and (d)). The calculated reaction energies and relevant barriers for  $O_2$  dissociation on the perfect and oxygen-deficient surfaces are collected in Table 4.

From Table 4, it can be clearly seen that the dissociation process of  $O_2$  on the perfect surface into P1 and P2 needs to overcome the energy barrier by 123.1 and 164.9 kJ mol<sup>-1</sup>, respectively. The reaction energies for the formation of P1 is exothermic by 82.4 kJ mol<sup>-1</sup>, whereas the reaction of P2 is endothermic by 84.8 kJ mol<sup>-1</sup>. The difference is 167.2 kJ mol<sup>-1</sup>. Consequently, the dissociation of  $O_2$  is thermodynamically favorable at  $Cu_{CUS}$  site leading to P1 but thermodynamically unfavorable resulting in P2, further implying that the dissociation of  $O_2$  into P2 is more feasible. Accordingly, the bond dissociation energy of free  $O_2$  molecule obtained by experiment is 504.7 kJ mol<sup>-1</sup> [56], it can be inferred that  $Cu_{CUS}$  site on the perfect surface has the efficient catalytic activity for  $O_2$  dissociation. For the deficient surface, the dissociation of  $O_2$  in the optimized M(d) structure leads to P3 with an activation energy of 82.4 kJ mol<sup>-1</sup>, furthermore, this reaction is highly exothermic by 245.0 kJ mol<sup>-1</sup>. The dissociation of  $O_2$  in the optimized M(e) and M(f) structures leads to P4, the activation energy is only 17.8 and 12.8 kJ mol<sup>-1</sup>, respectively. The corresponding reaction energies are also strongly exothermic by 209.4 and 198.7 kJ mol<sup>-1</sup>, respectively, further suggesting that the dissociation of  $O_2$  into P4 (one atomic oxygen is almost completely inserted into the crystal lattice and the other adsorbed at 3Cu site) is more feasible, which is in agreement with the experimental observation by Schulz and Cox [9].

Above reaction energies and relevant barriers show that a small quantity of  $O_2$  dissociation for M(d)–M(f) modes on the deficient surface leading to P4 is favorable both thermodynamically and kinetically in comparison with the dissociation of  $O_2$  on the perfect surface resulting in P1. The presence of oxygen vacancy can obviously improve the catalytic activity of  $Cu_2O$  for  $O_2$  dissociation, which is in agreement with the experimental results [9].

#### 4. Conclusions

A detailed density functional study with periodical slab calculations have been performed to illustrate the adsorption and dissociation of atomic and molecular oxygen on the perfect and deficient  $Cu_2O(111)$  surface. The optimized geometries, adsorption energies, vibrational frequencies and Mulliken charges show that atomic oxygen preferentially adsorbs at the threefold 3Cu site on the perfect surface and at the  $O_{vacancy}$  site on the deficient surface.  $Cu_{CUS}$  is the most advantageous adsorption site with molecularly adsorbed  $O_2$  lying flatly over singly coordinate  $Cu_{CUS}$ – $Cu_{CSA}$  bridge on the perfect surface, the oxygen species show the characteristic of the peroxy form ( $O_2^{2-}$ ). For the deficient surface, the dissociative adsorption is the main dissociation pathway of  $O_2$  on the  $Cu_2O(111)$  surface, and a small quantity of molecularly adsorbed  $O_2$  has been obtained. The dissociation

barrier of molecularly adsorbed  $O_2$  show that oxygen vacancy on the  $Cu_2O(111)$  surface exhibits strong catalytic activity for  $O_2$  dissociation in comparison with the dissociation of  $O_2$  on the perfect surface. Our calculation about the adsorption and dissociation of  $O_2$  on the  $Cu_2O(111)$  surface may provide some microscopic information for the catalytic mechanism of DMC synthesis over  $Cu_2O$  catalyst by the oxidative carbonylation of methanol.

#### Acknowledgements

The authors gratefully acknowledge the financial support of this study by the National Basic Research Program of China (2005CB221204) and the National Natural Science Foundation of China (20906066, 20976113 and 20976115).

#### References

- [1] S.A. Anderson, T.W. Root, J. Mol. Catal. A: Chem. 220 (2004) 247.
- [2] S.A. Anderson, T.W. Root, J. Catal. 217 (2003) 396.
- [3] Y.H. Zhang, I.J. Drake, D.N. Briggs, A.T. Bell, J. Catal. 244 (2006) 219.
- [4] Y.J. Wang, R.X. Jiang, X.Q. Zhao, S.F. Wang, J. Nat. Gas Chem. 9 (2000) 205.
- [5] S.T. King, Catal. Today 33 (1997) 173.
- [6] Z. Li, C.M. Wen, R.Y. Wang, H.Y. Zheng, K.C. Xie, Chem. J. Chin. Univ. 30 (2009) 2024.
- [7] Z. Li, C.M. Wen, R.Y. Wang, H.Y. Zheng, K.C. Xie, Chem. J. Chin. Univ. 31 (2010) 145.
- [8] R. Restori, D. Schwarzenbach, Acta Crystallogr. Sect. B 42 (1986) 201.
- [9] K.H. Schulz, D.F. Cox, Phys. Rev. B 43 (1991) 1610.
- [10] D. Le, S. Stolbov, T.S. Rahman, Surf. Sci. 603 (2009) 1637.
- [11] R.G. Zhang, B.J. Wang, L.X. Ling, H.Y. Liu, W. Huang, Appl. Surf. Sci. 257 (2010) 1175.
- [12] B.Z. Sun, W.K. Chen, Y. Li, C.H. Lu, Chin. J. Struct. Chem. 28 (2009) 311.
- [13] A. Soon, T. Söhnel, H. Idriss, Surf. Sci. 579 (2005) 131.
- [14] M.M. Islam, B. Diawara, V. Maurice, P. Marcus, J. Mol. Struct. (THEOCHEM) 903 (2009) 41.
- [15] B.Z. Sun, W.K. Chen, X. Wang, C.H. Lu, Appl. Surf. Sci. 253 (2007) 7501.
- [16] B.Z. Sun, W.K. Chen, J.D. Zheng, C.H. Lu, Appl. Surf. Sci. 255 (2008) 3141.
- [17] Z.J. Zuo, W. Huang, P.D. Han, Z.H. Li, Appl. Surf. Sci. 256 (2010) 2357.
- [18] U. Romano, R. Tesel, M.M. Mauri, P. Rebora, Ind. Eng. Chem. Prod. Res. Dev. 19 (1980) 396.
- [19] I.J. Drake, Y.H. Zhang, D. Briggs, B. Lim, T. Chau, A.T. Bell, J. Phys. Chem. B 110 (2006) 11654.
- [20] S.T. King, J. Catal. 161 (1996) 530.
- [21] X.B. Zheng, A.T. Bell, J. Phys. Chem. C 112 (2008) 5043.
- [22] R.G. Zhang, H.Y. Zheng, B.J. Wang, Z. Li, Chem. J. Chin. Univ. 31 (2010) 1246.
- [23] V.E. Heinrich, P.A. Cox, The Surface Science of Oxides, Cambridge University Press, Cambridge, 1994.
- [24] M. Witko, J. Mol. Catal. 70 (1991) 277.
- [25] L.N. Kantorovich, M.J. Gillan, Surf. Sci. 374 (1997) 373.
- [26] E.R.C. Winter, J. Chem. Soc. (London) (1968) A2889.
- [27] G.K. Borekov, Discuss. Faraday Soc. 41 (1966) 263.
- [28] M. Che, A.J. Tench, Adv. Catal. 32 (1983) 1.
- [29] T. Yang, X.D. Wen, C.F. Huo, Y.W. Li, J.G. Wang, H.J. Jiao, J. Mol. Catal. A: Chem. 30 (2009) 129.
- [30] P. Lukinskas, D. Fărcașiu, Appl. Catal. A: Gen. 209 (2001) 193.
- [31] A. Sierralta, O. Lisboa, L. Rodriguez, J. Mol. Struct. (THEOCHEM) 729 (2005) 91.
- [32] M.Y. Sun, A.E. Nelson, J. Adjaye, J. Catal. 233 (2005) 411.
- [33] M. Pozzo, D. Alfè, Int. J. Hydrogen Energy 34 (2009) 1922.
- [34] Y.J. Xu, J.Q. Li, Y.F. Zhang, W.K. Chen, Acta Phys. Chim. Sin. 19 (2003) 414.
- [35] F.R. Sensato, R. Custódio, M. Calatayud, A. Beltrán, J. Andrés, J.R. Sambrano, E. Longo, Surf. Sci. 511 (2002) 408.
- [36] M.S. Palmer, M. Neurock, M.M. Olken, J. Phys. Chem. B 106 (2002) 6543.
- [37] M.P.D. Lara-Castells, J.L. Krause, Chem. Phys. Lett. 354 (2002) 483.
- [38] S. Wendt, R. Schaub, J. Matthiesen, E.K. Vestergaard, E. Wahlström, M.D. Rasmussen, P. Thosttrup, L.M. Molina, E. Lægsgaard, I. Stensgaard, B. Hammer, F. Besenbacher, Surf. Sci. 598 (2005) 226.
- [39] B.Z. Sun, W.K. Chen, X. Wang, Y. Li, C.H. Lu, Chin. J. Inorg. Chem. 24 (2008) 340.
- [40] V. Maurice, H.H. Strehblow, P. Marcus, Surf. Sci. 458 (2000) 185.
- [41] J. Kunze, V. Maurice, L.H. Klein, H.H. Strehblow, P. Marcus, J. Phys. Chem. B 105 (2001) 4263.
- [42] J. Kunze, V. Maurice, L.H. Klein, H.H. Strehblow, P. Marcus, Electrochim. Acta 48 (2003) 1157.
- [43] J.P. Perdew, J.A. Chevary, S.H. Vosko, K.A. Jackson, M.R. Pederson, D.J. Singh, C. Fiolhais, Phys. Rev. B 46 (1992) 6671.
- [44] P. Hu, D.A. King, S. Crampin, M.H. Lee, M.C. Payne, Chem. Phys. Lett. 230 (1994) 501.
- [45] A.D. Becke, J. Chem. Phys. 88 (1988) 2547.
- [46] C. Lee, W. Yang, R.G. Parr, Phys. Rev. B 37 (1988) 785.
- [47] M. Dolg, U. Wedig, H. Stoll, H. Preuss, J. Chem. Phys. 86 (1987) 866.

- [48] A. Bergner, M. Dolg, W. Kuechle, H. Stoll, H. Preuss, *Mol. Phys.* 80 (1993) 1431.
- [49] Y. Inada, H. Orita, *J. Comput. Chem.* 29 (2008) 225.
- [50] T.A. Halgren, W.N. Lipscomb, *Chem. Phys. Lett.* 49 (1977) 225.
- [51] B. Delley, *J. Chem. Phys.* 92 (1990) 508.
- [52] B. Delley, *J. Chem. Phys.* 113 (2000) 7756.
- [53] D.R. Lide, *Handbook of Chemistry and Physics*, 82nd ed., CRC Press, Boca Raton, 2001.
- [54] M.A. Nygren, L.G.M. Pettersson, *J. Phys. Chem.* 100 (1996) 1874.
- [55] K. Nakamoto, *Infrared and Raman Spectra of Inorganic and Coordination Compounds*, 4th ed., John Wiley and Sons Press, New York, 1986.
- [56] J.P. Perdew, K. Burke, M. Ernzerhof, *Phys. Rev. Lett.* 77 (1996) 3865.